SCIENTIFIC REPORTS

OPEN

SUBJECT AREAS:
NANOWIRES
NANOSCIENCE AND TECHNOLOGY

Received
7 November 2014

Accepted
14 November 2014

Published
11 December 2014

Correspondence and requests for materials should be addressed to X.Z. (xinyi.zhang@monash.edu) or D.R.M. (douglas.macfarlane@monash.edu)

Nanofabrication of highly ordered, tunable metallic mesostructures via quasi-hard-templating of lyotropic liquid crystals

Xinyi Zhang[1], Wei Lu[2], Jiyan Dai[2], Laure Bourgeois[3], Jianfeng Yao[4], Huanting Wang[4], James R. Friend[5], Dongyuan Zhao[4] & Douglas R. MacFarlane[1]

[1]School of Chemistry, Monash University, Clayton, VIC3800, Australia, [2]Department of Applied Physics and Materials Research Centre, The Hong Kong Polytechnic University, Kowloon, Hong Kong, P.R. China, [3]Monash Centre For Electron Microscopy and Department of Materials Engineering, Monash University, Clayton, VIC3800, Australia, [4]Department of Chemical Engineering, Monash University, Clayton, VIC3800, Australia, [5]Micro/Nanophysics Research Laboratory, RMIT University, Melbourne, VIC 3000 (Australia).

The synthesis of metal frameworks perforated with nanotunnels is a challenge because metals have high surface energies that favor low surface area structures; traditional liquid-crystal templating techniques cannot achieve the synthetic control required. We report a synthetic strategy to fabricate metal nanomaterials with highly ordered, tunable mesostructures in confined systems based on a new quasi-hard-templating liquid-crystals mechanism. The resulting platinum nanowires exhibit long range two-dimensional hexagonally ordered mesopore structures. In addition, single crystalline hexagonal mesoporous platinum nanowires with dominant {110} facets have been synthesized. Finally, we demonstrate that the mesostructures of metal nanomaterials can be tuned from hexagonal to lamellar mesostructures.

Nanoporous metals represent a class of material with characteristics contrasting with those of the conventional bulk, thin film and nanocrystalline forms. These materials demonstrate rich physical and chemical properties and functions that largely depend on their pore size and architectures[1–4]. Engineering their structure at the mesoscale is critical for their application in sensors, batteries, fuel cells, data storage, computation, plasmonics and metamaterial devices[5–13].

Self-assembled lyotropic liquid crystals (LLCs) have long been used as soft templates for synthesizing ordered mesoporous materials including silica, semiconductors, and metals[14–20]. In these techniques, the surfactants, inorganic or metal precursors, and solvents are mixed together, followed by the self-assembly of the surfactants into LLCs under different circumstances. For example, mesostructured silica is prepared through evaporation-induced self-assembly. This methodology involves electrostatic interactions and charge matching at the interface of the self-assembled surfactant molecules and ionic silica precursors[21]. Compared to siliceous materials, the synthesis of ordered mesoporous metals is more difficult, because metals have high surface energies that favour low surface area structures[22]. Interestingly, despite this important difference, the traditional starting procedure for preparing mesoporous metals is quite similar to those for silica mesostructures. In the synthesis of mesoporous metals, the metal species are first mixed with surfactant and water, followed by vigorous stirring and several heating/cooling cycles in order to obtain a homogeneous LLC phase; the main difference is that highly concentrated surfactants and metal compounds are used without dilution and the self-assembly is induced by temperature[19,20]. A number of limitations to these current LLC templating techniques thus emerge: (1) The highly concentrated metal ions, especially noble metal ions, are not stable during the heating/cooling cycles, and reduction may happen before the formation of the LLCs. (2) The interaction between the metal ions and the surfactants may lead to the random nucleation of nanoparticles and the obtained mesoporous metals are therefore often composed of aggregated nanoparticles. It is difficult to synthesize high-crystallinity, or even single-crystal metal mesostructures, in these ternary mixture systems. (3) The preparation of ordered mesoporous metals in confined systems remains elusive, due to the high viscosity of the ternary mixture, especially for some

LLC mesophases such as the lamellar mesophase, which require even higher concentrations of surfactants[23]. Some progress has been made[24–26]. For example, Yamauchi et al. prepared Pt nanofibers with stacked donut-like mesostructures composed of aggregated nanoparticles from diluted precursor solutions via an evaporation-mediated direct templating method[25]. However, major challenges remain in the development of ordered mesoporous metals with controllable geometry and structure.

Here, we report a general strategy for the fabrication of nanostructured metals with highly ordered mesoporosity in a confined system. In order to obtain homogenous mesophases and avoid the metal ion related issues, we prepared the LLCs from binary octaethylene glycol monohexadecyl ether ($C_{16}EO_8$)–H_2O systems. The binary $C_{16}EO_8$–H_2O solutions can self-assemble into homogenous LLCs with tunable mesophases, from hexagonal to lamellar structures, by adjusting the concentration. We found that the obtained binary LLCs are stable and persistent and can be utilized as a hard template in the formation of metallic mesostructures. Therefore, the cooperative assembly between the surfactant and metal species is not necessary to achieve the metallic mesostructures and hence we refer to these LLC systems as "quasi-hard templates". By using the cylindrical nanochannels of anodic aluminium oxide (AAO) as confined systems, we demonstrate that metal nanostructures with controlled composition and geometry and tunable mesostructure can be accomplished by direct electrodeposition using these preformed binary LLCs as quasi-hard templates.

Mesoporous platinum nanostructures were fabricated by first preparing hexagonal LC mesophases in cylindrical nanochannels of AAO followed by the electrodeposition of the metal. The success of this strategy depends on the preparation of homogeneous LLCs in AAO. The details of the procedure are shown in experimental and Figure S1 in Supplementary Information. The small angle XRD pattern for the LLCs prepared with binary $C_{16}EO_8$–H_2O solution shows three peaks (Figure S2 in Supplementary Information) that are indexable as (100), (110), and (200) reflections, revealing the formation of highly ordered hexagonal (p6mm) mesostructure. Figure 1 shows transmission electron microscopy (TEM) images and the corresponding electron diffraction (ED) patterns of the resultant Pt nanowires with diameters of 50 nm. The bright rings can be indexed as the face-centered cubic (FCC) Pt structure (Figure 1a, inset). The ordered mesopores are visible on the surface of a bundle of Pt nanowires (Figure 1b), and the corresponding ED pattern [Figure 1b, inset] reveals a dominant crystallographic orientation that could be indexed as the [110] zone axis of face-centered cubic platinum structure. A high magnification TEM image of the mesoporous Pt nanowire is displayed as Figure 1c, where hexagonal arranged mesopores with pore size about 3 nm and interpore distance about 6 nm can be clearly observed, which is consistent with the lattice parameter (~ 6 nm) of the hexagonal mesophase of $C_{16}EO_8$ LLC[18]. The highly ordered, hexagonally organized mesostructure of the Pt nanowires suggests that the $C_{16}EO_8$ molecules self-assembled into hexagonal mesophase with LC rods perpendicularly aligned on the nanochannel walls of AAO and the resulting LLC mesophases are stable and maintained during the deposition of Pt nanowires. The corresponding ED pattern can be indexed as single crystalline Pt nanowire oriented along the [110] direction. The nature of the single-crystal structure of the Pt nanowires and their growth orientation were further confirmed by high-resolution TEM (HRTEM). The HRTEM images and corresponding Fourier transforms displayed in Figure 1e–1f show clearly the single-crystal nature of the Pt nanowires with orientations along the [110] directions. The well-resolved lattice spacings of 0.22 nm and 0.20 nm correspond to the Pt {111} and {200} atomic planes, respectively. The mesopores are normal to the surface of the Pt nanowires. These mesopores are not exactly parallel to the electron beam because of the curved surface, therefore the lattice fringes of the mesopore walls can be observed. The surface of the single-crystalline mesoporous nanowires can be identified as the {110} planes of FCC Pt structure. It is worth noting that the HRTEM image of two mesoporous Pt nanowires shows that both Pt nanowires exhibit single crystal structures with {110} facets (Figure 1e). The porosity of mesoporous Pt nanowires is calculated from nitrogen sorption results to be 35.6%. The pore size distributions of the samples are observed to be narrow and the corresponding peak is located at about 2.9 nm (Figure S3 in the Supplementary Information).

The structure of the mesoporous Pt nanowires is illustrated in Figure 2. The long range two-dimensional hexagonally ordered mesoporous structure of Pt nanowire is directly evidenced by TEM

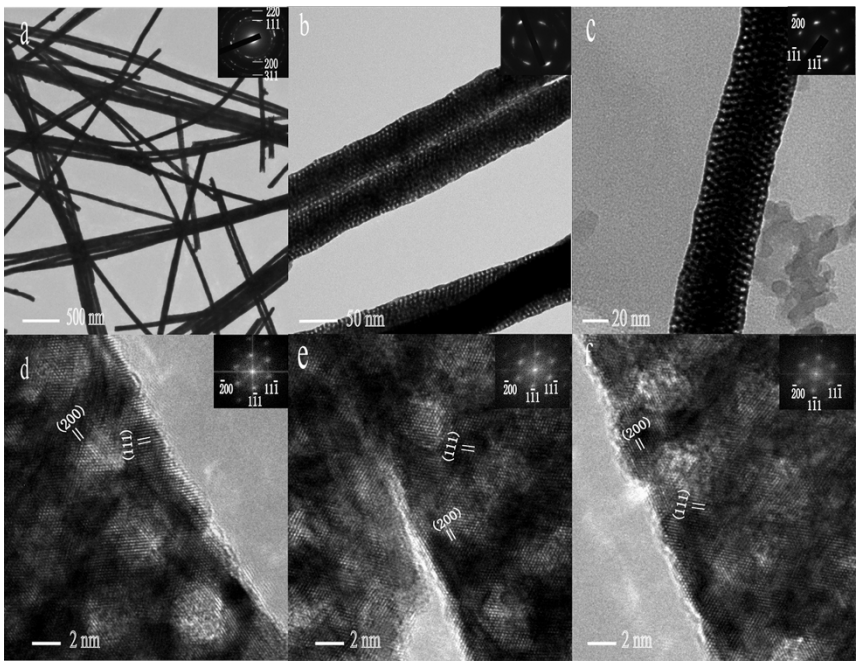

Figure 1 | Mesoporous Pt nanowires with diameters about 50 nm: (a,b,c) TEM images with different magnification and the corresponding electron diffraction patterns (insets). (d,e,f) HRTEM images of the mesoporous Pt nanowires and the corresponding Fourier transform patterns (insets).

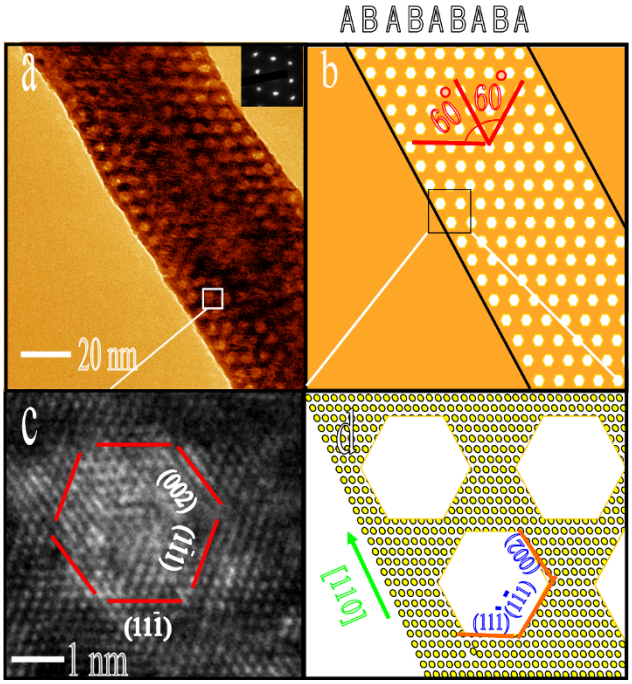

Figure 2 | The structures of the mesoporous Pt nanowire: (a) TEM image of the Pt nanowire and the corresponding electron diffraction patterns (insets). (b) Reconstructed image of Figure 2a. (c) HRTEM of a mesopore. (d) Modelling of crystal structure of the mesoporous Pt nanowire.

(Figure 2a). There are three types of rows of close packed mesopores: one is the longitudinal rows arranged in an A-B-A-B stacking pattern, in which the mesopores are aligned parallel to the axis of the nanowires (see also Figure S4 in the Supplementary Information). The other two types of rows are intersecting helicies with angles of $\pm$ 60° to the axis of the nanowires, respectively. In a confined geometry, the phase behaviour of liquid crystals is considerably affected by the curvature effects and the interaction between the LCs and the channel wall. The structure adopted is therefore a balance between micelle-wall and intermicellar interaction. In a cylindrical channel, the surface (or interface) stresses include axial stress and hoop stress, and the latter is much larger than the former[27]. The curvature effects are mainly caused by the hoop stress perpendicular to the axis of the channels. The A-B-A-B arrangement allows the highest density in each row along the longitudinal section of the AAO channels and the lowest density in the direction along the cross-section of the AAO channels. In each longitudinal row, all the LLC rods are in the same longitude. Such arrangement minimizes the stress caused by the curvature effects.

For the FCC structure, the surface energies associated with the low-index crystallographic planes are in the order of $\gamma_{(111)} < \gamma_{(100)} < \gamma_{(110)}$[28]. Therefore, a Pt nanocrystal with {111} facets should be more stable than that with {110} facets. However, according to the observation by TEM, these mesoporous Pt nanowires have dominant {110} facets. In general, the grains with the fastest growing facet facing the growth direction then dominate via a competition and coalescence process. For the mesoporous nanowires, the existence of the nanochannel walls and LLC rods should play important roles in the grain competition. The LLC rods in particular generate a large amount of inner mesoporous walls, the area fraction of which is larger than that of the nanowire surface. This will also impact on the growth of the mesoporous nanowires. As shown in Figures 2c and 2d, the mesoporous walls may contain a large amount of inner {111} facets, which are energetically preferred. The growth form that the mesoporous Pt nanowires adopted is the balance of the interactions among the metal grains and LLC rods and AAO nanochannel walls.

In the LLC loaded AAO template, the deposition rate of platinum is very slow due to the low diffusion rate of platinum ions in the nanovoids. When the concentration of metal species drops below the minimum concentration for nucleation, the nucleation stops whereas the growth continues. The critical nucleus radius for homogeneous metal nucleation can be calculated from[29]:

$$r^* = -2\gamma/\Delta G_v \quad (1)$$

$$\Delta G_v = -\mathrm{kT}/\Omega \ln(\mathrm{C}/\mathrm{C}_0) \quad (2)$$

where γ is the surface energy per unit area, ΔG_v is the change of Gibbs free energy, C is the concentration of the solute, C_0 is the equilibrium concentration or solubility, Ω is the atomic volume. It can be seen that the critical radius of the metal nucleus mainly depends on the surface energy and the concentration of the metal ions. Given the small size of the voids between the LLC rods and the low diffusion rate of Pt ions in the voids, it is reasonable to assume that the formation of new nuclei becomes difficult during the Pt deposition. In this situation, the oriented growth of existing grains could be thermodynamically favourable in comparison with the nucleation of new grains. We believe that the confinement of the narrow nanovoids in the LLC loaded AAO template and the low growth rate at low temperature are the main factors behind the formation of the single crystalline platinum nanowires. When the deposition reaches the LLC rods, these ultrathin LLC rods can be embedded without changing the structural continuity of the matrix, resulting in the single crystalline structure of the mesoporous Pt nanowires.

The formation of stable LLCs inside of the AAO nanochannels is the crucial step for the fabrication of mesoporous Pt nanowires. A key question is whether the confinement effects might change the molecular assembly and lead to new mesostructures as a function of the pore diameter of the AAO. Therefore, mesoporous Pt nanostructures were fabricated by using AAO templates with different pore sizes. Figure 3 shows the TEM images of mesoporous Pt nanowires prepared by using AAO templates with diameters from 45 nm to about 85 nm. All Pt nanowires exhibit long range two-dimensional hexagonally ordered mesoporous structures, confirming the formation of stable hexagonal LCs inside the cylindrical nanochannels. Again, the assemblies of the LLC mesophases obey the A-B-A-B stacking pattern within the pore diameter range.

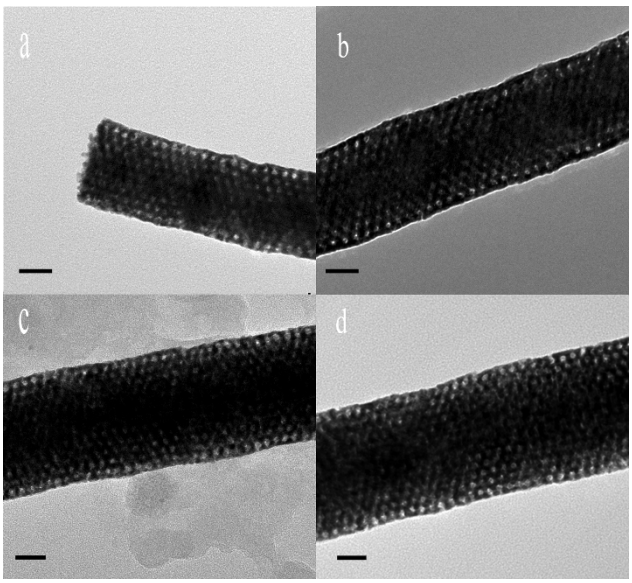

Figure 3 | **TEM images of the mesoporous Pt nanowires prepared by using AAO templates with different pore diameters: (a) 45 nm, (b) 60 nm, (c) 76 nm, (d) 85 nm.** Scale bar, 20 nm.

Controlling the structure and orientation of mesoporous channels is of great interest for many applications. According to the binary $C_{16}EO_8$/water phase diagram, a lamellar phase occurs at volume fractions above the close-packing limit of rods micelles[30,31]. So inverted lamellar metal mesostructures can be designed and fabricated through LC templating. Figure 4 shows the TEM images of Pt and Co nanowires prepared from AAO template with pore diameter ~ 45 and 55 nm by using a 70 wt% $C_{16}EO_8$ solution, respectively. Stacked multilayers with layered mesoporous channels of several hundreds of nanometers can be observed on both of the Pt and Co nanowires, and the mesochannels are predominantly oriented parallel to the cavity walls of the AAO templates. As shown in the corresponding ED patterns, both Pt and Co nanowires possess FCC structures. The thickness of the layers and interchannel distance of the lamellar mesostructures are about 2~4 and 3~5 nm, respectively. The interlayer distance of the lamellar mesostructured Pt nanowire is smaller than the interpore distance of the hexagonal mesoporous Pt nanowires, revealing a higher packing density of the lamellar mesophase in comparison with the hexagonal mesophase. Figures 4e and 4f show the HRTEM images of lamellar mesostructured Pt and Co nanowires, respectively. The Pt{111}, Pt{200}, and Pt{220} and Co{111} lattice fringes with respective spacings of 0.22, 0.20, and 0.14 nm and 0.20 nm are visible.

The formation of the metal mesostructures is illustrated in Figure 5. The stability of the LLCs is critical for the preparation of metal mesostructures. The LLCs are formed by the aggregation of hundreds of amphilic molecules into large anisotropic micelles through intermicellar interaction inducing an entropy-driven phase transition, while the alignment of LCs is due to the interaction between the LC molecules and the substrate. The regular mesostructures of the metal nanowires reveals that the perpendicular orientation of the surface alignment produced ordered layers on the cylindrical walls of the AAO templates. It is well known that the alignment orientation of LCs can be determined by the substrate; this phenomenon of orientation of liquid crystals by a surface has been described as "anchoring"[32,33]. The homeotropic alignment of LLCs can be achieved on plasma-treated substrate[34], confined surface[35] or by an external field[36]. The LC alignment perpendicular to the substrates is favourable here because of the attraction between the electronegative EO groups[37] and the positive charge the AAO channel walls[38]. The confinement effect should play an important role in the homeotropic alignment of LLCs on of the AAO channel walls[39]. The steric confinement of channels may also restrict the movement of LC micelles. Therefore, the cylindrical channels not only contribute to the alignment of the LCs but also increase the stability of the LC mesophase. Thus the stabilized LLCs within the AAO channels can

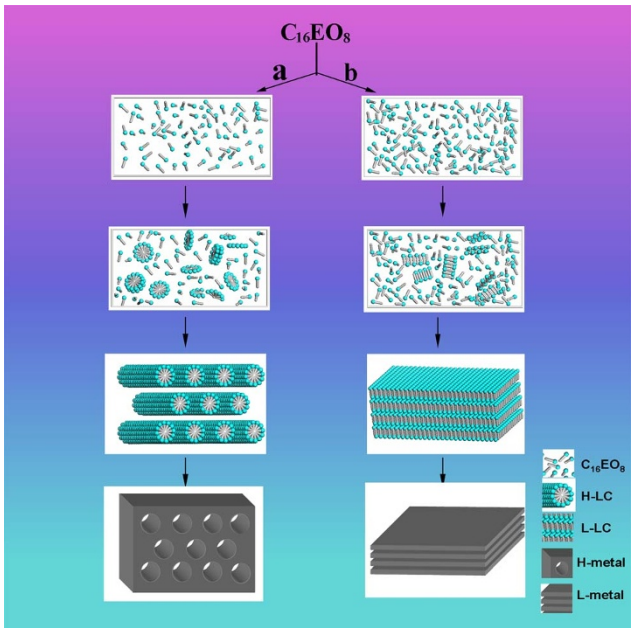

Figure 5 | Schematic illustration of the preparation of mesostructured metals by using $C_{16}EO_8$ at concentration of (a) 55 wt% and (b) 70 wt%.

serve as a "hard template" during the deposition of ordered mesoporous metals. Under such conditions, one might expect similar self-assembly behaviours repeatable in other confined nanosystems.

In summary, we have developed a general strategy for the nanofabrication of highly ordered mesostructured metals via quasi-hard-templating of LLCs in a confined system. We demonstrate that stable and homogenous binary mesophases formed inside the nanochannels of AAO can act as a hard template for the synthesis of metal mesostructures. Particularly, single crystalline hexagonal mesostructured platinum nanowires with dominant {110} facets have been fabricated. Such single crystal nanomaterials can offer ideal model systems for reliable study of their material properties. For example, mesoporous Pt nanowires with dominant {110} facets show promises for applications in fuel cells since the activity for oxygen reduction reaction on {110} of Pt is known to be the highest among low-index crystallographic planes[40,41]. Besides, the single crystal structure of the nanowires can avoid the issues caused by grain boundaries and may have applications in novel electronic nanodevices. In addition, the highly ordered mesopores in the metal nano-

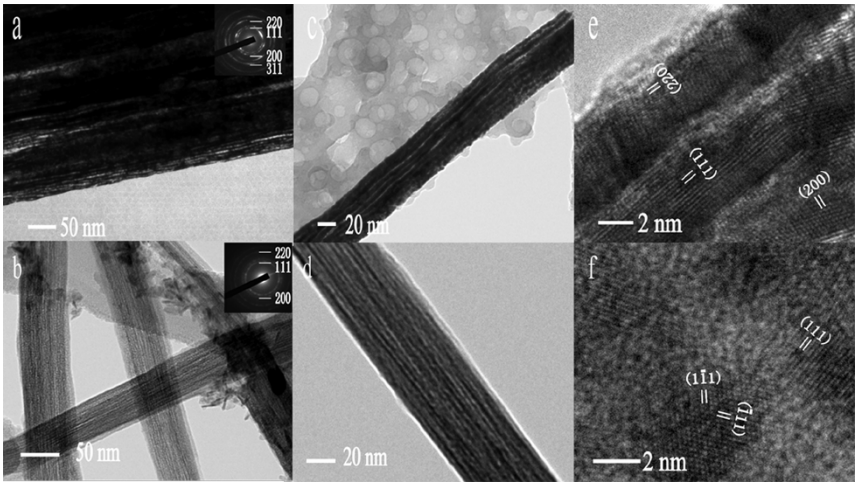

Figure 4 | TEM images of lamellar mesostructured Pt (a, c, e) and Co (b, d, f) nanowires and the corresponding electronic diffraction patterns.

wires can lead to uniform localized electromagnetic field enhancement and generate uniformly distributed "hot spots"[42]. Thus, these materials may have application in extra-sensitive, repeatable surface-enhanced Raman spectroscopy. The present method provides a way not only to fabricate ordered mesoporous metals in confined nanosystem, but also to control the geometry, orientation, and structures. We expect that this work can help to establish a new mechanistic understanding of the formation of metal mesostructures and may be generalized to the LLC templating synthesis of other materials.

1. Erlebacher, J., Aziz, M. J., Karme, A., Dimitrov, N. & Sieradzki, K. Evolution of nanoporosity in dealloying. *Nature* **410**, 450–453 (2001).
2. Weissmüller, J. *et al*. Charge-induced reversible strain in a metal. *Science* **300**, 312–315 (2003).
3. Lefebvre, L.-P., Banhart, J. & Dunand, D. C. Porous metals and metallic foams: current status and recent developments. *Adv. Eng. Mater.* **10**, 775–785 (2010).
4. Warren, S. C. *et al*. Ordered mesoporous materials from metal nanoparticles-block copolymer self-assembly. *Science* **320**, 1748–1752 (2008).
5. Yamauchi, Y. & Kuroda, K. Rational design of mesoporous metals and related nanomaterials by a soft-template approach. *Chem. Asian J.* **3**, 664–676 (2008).
6. Wu, Y. Y. *et al*. Composite mesostructures by nano-confinement. *Nature Mater.* **3**, 816–822 (2004).
7. Li, C. L., Sato, T. & Yamauchi, Y. Electrochemical synthesis of one-dimensional mesoporous Pt nanorods using the assembly of surfactant micelles in confined space. *Angew. Chem. Int. Ed.* **52**, 8050–8053 (2013).
8. Fujita, T. *et al*. Atomic origins of the high catalytic activity of nanoporous gold. *Nature Mater.* **11**, 775–780 (2012).
9. Chan, S., Kwon, S., Koo, T., Lee, L. P. & Berlin, A. A. Surface-enhanced Raman scattering of small molecules from silver-coated silicon nanopores. *Adv. Mater.* **15**, 1595–1598 (2003).
10. Baumberg, J. J. *et al*. Angle-resolved surface-enhanced Raman scattering on metallic nanostructured plasmonic crystals. *Nano Lett.* **5**, 2262–2267 (2005).
11. Fujita, T., Okada, H., Koyama, K., Watanabe, K., Maekawa, S. & Chen, M. W. Unusually small electrical resistance of three-dimensional nanoporous gold in external magnetic fields. *Phys. Rev. Lett.* **101**, 166601 (2008).
12. Biener, J., Nyce, G. W., Hodge, A. M. & Biener, M. M. Nanoporous plasmonic metamaterials. *Adv. Mater.* **20**, 1211–1217 (2008).
13. Yu, F., Ahl, S., Caminade, A. M., Majoral, J. P., Knoll, W. & Erlebacher, J. Simultaneous excitation of propagating and localized surface plasmon resonance in nanoporous gold membranes. *Anal. Chem.* **78**, 7346–7350 (2006).
14. Kresge, C. T., Leonowicz, M. E., Roth, W. J., Vartuli, J. C. & Beck, J. S. Ordered mesoporous molecular-sieves synthesized by a liquid-crystal templating mechanism. *Nature* **359**, 710–712 (1992).
15. Beck, J. S. *et al*. A new family of mesoporous molecular-sieves prepared with liquid-crystal templates. *J. Am. Chem. Soc.* **114**, 10834–10843 (1992).
16. Johnson, S. A., Ollivier, P. J. & Mallouk, T. E. Ordered mesoporous polymers of tunable pore size from colloidal silica templates. *Science* **283**, 963–965 (1999).
17. Zhao, D. Y. *et al*. Triblock copolymer syntheses of mesoporous silica with periodic 50 to 300 angstrom pores. *Science* **279**, 548–552 (1998).
18. Braun, P. V., Osenar, P., Twardowski, M., Tew, G. N. & Stupp, S. I. Macroscopic nanotemplating of semiconductor films with hydrogen-bonded lyotropic liquid crystals. *Adv. Funct. Mater.* **15**, 1745–1750 (2005).
19. Attard, G. S. *et al*. Mesoporous platinum films from lyotropic liquid crystalline phases. *Science* **278**, 838–840 (1997).
20. Attard, G. S., Gőltner, C. G., Corker, J. M., Henke, S. & Templer, R. H. Liquid-crystal templates for nanostructured metals. *Angew. Chem. Int. Ed.* **36**, 1315–1317 (1997).
21. Brinker, C. J., Lu, Y. F., Sellinger, A. & Fan, H. Y. Evaporation-induced self-assembly: Nanostructures made easy. *Adv. Mater.* **11**, 7, 579–585 (1999).
22. Warren, S. C. & Wiesner, U. Self-assembled ordered mesoporous metals. *Pure Appl. Chem.* **81**, 73–84(2009).
23. Attard, G. S., Bartlett, P. N., Coleman, N. R. B., Elliott, J. M. & Owen, J. R. Lyotropic liquid crystalline properties of nonionic surfactant/H_2O/hexachloroplatinic acid ternary mixtures used for the production of nanostructured platinum. *Langmuir* **14**, 7340–7342 (1998).
24. Takai, A., Yamauchi, Y. & Kuroda, K. Tailored electrochemical synthesis of 2D-hexagonal, lamellar, and cage-type mesostructured Pt thin films with extralarge periodicity. *J. Am. Chem. Soc.* **132**, 208–214 (2010).
25. Yamauchi, Y., Takai, A., Nagaura, T., Inoue, S. & Kuroda, K. Pt fibers with stacked donut-like mesospace by assembling Pt nanoparticles: guided deposition in physically confined self-assembly of surfactants. *J. Am. Chem. Soc.* **130**, 5426–5427 (2008).
26. Zhang, X. Y. *et al*. Ordered hierarchical porous platinum membranes with tailored mesostructures. *Angew. Chem. Int. Ed.* **49**, 10101–10105 (2010).
27. Adams, N. J. I. Seismic design rules for flat bottom cylindrical liquid storage tanks. *Int. J. Pres. Ves. Pip.* **49**, 61–69 (1992).
28. Wang, Z. L. Transmission electron microscopy of shape-controlled nanocrystals and their assemblies. *J. Phys. Chem. B* **104**, 1153–1175 (2000).
29. Matijević, E. Production of monodispersed colloidal particles. *Ann. Rev. Mater. Sci.* **15**, 483–516 (1985).
30. Mitchell, D. J., Tiddy, G. J., Waring, L., Bostock, T. & McDonald, M. P. Phase-behavior of polyoxyethylene surfactants with water-mesophase structures and partial miscibility (cloud points). *J. Chem. Soc. Faraday Trans.* **79**, 975–1000 (1983).
31. Miller, C. A. & Raney, K. H. Solubilization emulsification mechanisms of detergency. *Colloids Surf. A* **74**, 169–215 (1993).
32. Jérôme, B. Surface effects and anchoring in liquid-crystals. *Rep. Prog. Phys.* **54**, 391–451 (1991).
33. Crawford, G. P., Stannarius, R. & Doane, J. W. Surface-induced orientational order in the isotropic-phase of a liquid-crystal material. *Phys. Rev. A* **44**, 2558–2569 (1991).
34. Shahidzadeh, N., Merdas, A. & Urbach, W. Orientation of Lyotropic and Thermotropic Liquid Crystals on Plasma-Treated Fluorinated Surfaces. *Langmuir* **14**, 6594–6598 (1998).
35. Jayasri, D., Sairam, T., Murthyc, K. P. N. & Sastry, V. S. S. Liquid crystal films on curved surfaces: An entropic sampling study. *Physica A* **390**, 4549–4554 (2011).
36. Oliveira, E. A. & Figueiredo, N. A. M. Anchoring properties of lyotropic liquid crystals near the nematic-isotropic transition. *Phys. Rev. E* **49**, 629 (1994).
37. Bakshi, M. S., Sachar, S., Yoshimura, T. & Esumi, K. Association behavior of poly(ethylene oxide)-polypropylene oxide)poly(ethylene oxide) block copolymers with cationic surfactants in aqueous solution. *J. Colloid Interf. Sci.* **278**, 224–233 (2004).
38. Miao, J. Y. *et al*. Micropumps based on the enhanced electroosmotic effect of aluminum oxide membranes. *Adv. Mater.* **19**, 4234–4239 (2007).
39. Crawford, G. P., Yang, D. K., Zumer, S., Finotello, D. & Doane, J. W. Ordering and self-diffusion in the first molecular layer at a liquid-crystal-polymer interface. *Phys. Rev. Lett.* **66**, 723–726 (1991).
40. Markovic, N. M., Gasteiger, H. & Ross, P. N. Kinetics of oxygen reduction on Pt (hkl) electrodes: Implications for the crystallite size effect with supported Pt electrocatalysts. *J. Electrochem. Soc.* **144**, 1591–1597 (1997).
41. Grgur, B. N., Markovic, N. M. & Ross, P. N. Temperature dependent oxygen electrochemistry on platinum low index single crystal surfaces in acid solutions. *Can. J. Chem.* **75**, 1465–1471 (1997).
42. Liu, H. W. *et al*. Single molecule detection from a large-scale SERS-active $Au_{79}Ag_{21}$ substrate. *Sci. Rep.* **1**, 112 (2011).

Acknowledgments

This work was supported by the Australian Research Council through Grant No.: DP120104334 and DP120101194 and through DRM's Australian Laureate Fellowship. This work was performed in part at the Melbourne Centre for Nanofabrication (MCN) in the Victorian Node of the Australian National Fabrication Facility (ANFF). The authors acknowledge use of facilities within the Monash Centre for Electron Microscopy.

Author contributions

X.Z. and D.M. conceived the experiments. X.Z., J.Y. and W.L. prepared the samples. W.L., J.D. and L.B. performed TEM analysis. H.W., J.F. and D.Z. contributed to the interpretation of experiments. X.Z. and D.M. prepared the manuscript. All the authors discussed the results and commented on the manuscript.

Additional information

Supplementary information accompanies this paper at http://www.nature.com/scientificreports

Competing financial interests: The authors declare no competing financial interests.

How to cite this article: Zhang, X. *et al*. Nanofabrication of highly ordered, tunable metallic mesostructures via quasi-hard-templating of lyotropic liquid crystals. *Sci. Rep.* **4**, 7420; DOI:10.1038/srep07420 (2014).

This work is licensed under a Creative Commons Attribution-NonCommercial-ShareAlike 4.0 International License. The images or other third party material in this article are included in the article's Creative Commons license, unless indicated otherwise in the credit line; if the material is not included under the Creative Commons license, users will need to obtain permission from the license holder in order to reproduce the material. To view a copy of this license, visit http://creativecommons.org/licenses/by-nc-sa/4.0/